ACS APPLIED MATERIALS & INTERFACES

Research Article

www.acsami.org

Interface Effects on the Electronic Transport Properties in Highly Epitaxial $LaBaCo_2O_{5.5+\delta}$ Films

C. R. Ma,[†] M. Liu,[‡] J. Liu,[†] G. Collins,[†] Y. M. Zhang,[†] H. B. Wang,[†] C. L. Chen,*[,†] Y. Lin,[§] J. He,[⊥] J. C. Jiang,[⊥] E. I. Meletis,[⊥] and A. J. Jacobson[∥]

[†]Department of Physics and Astronomy, University of Texas at San Antonio, San Antonio, Texas 78249, United States

[‡]Electronic Materials Research Laboratory and International Center for Dielectric Research, Xi'an Jiaotong University, Xi'an, Shaanxi 710049, People's Republic of China

[§]State Key Laboratory of Electronic Thin Films and Integrated Devices, University of Electronic Science & Technology of China, Chengdu, Sichuan 610054, People's Republic of China

[⊥]Department of Materials Science and Engineering, University of Texas at Arlington, Arlington, Texas 76019, United States

[∥]Department of Chemistry, University of Houston, Houston Texas 77204, United States

ABSTRACT: Single-crystalline perovskite $LaBaCo_2O_{5.5+\delta}$ thin films were grown on a (110) $NdGaO_3$ single-crystal substrate in order to systematically investigate the effect of lattice mismatch on the electrical transport properties in comparison to the films on $LaAlO_3$, $SrTiO_3$, and MgO substrates. Microstructure studies reveal that all of the $LaBaCo_2O_{5.5+\delta}$ films are of excellent quality with atomically sharp interface structures. The electrical and magnetic transport property studies indicate that the resistivity, magnetoresistance, and magnetic moment of the film are very sensitive to the substrate materials because of the lattice mismatch/interface strain. The Curie temperature, however, is almost independent of the strain imposed by the substrate, probably because of the strong coupling between the nanodomain boundary and interface strain.

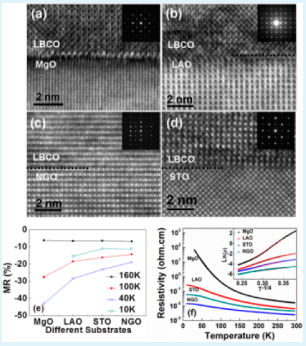

KEYWORDS: *$LaBaCo_2O_{5.5+\delta}$ thin films, interface strain, magnetoresistance*

INTRODUCTION

Perovskite cobaltates have attracted great attention not only for their important mixed ionic/electronic conductivity behavior but also because of their interesting magnetic transport properties.[1−4] Among them, the $LnBaCo_2O_{5.5+\delta}$ (Ln = La, Pr, Gd, Tb, Dy, Ho) family has shown various exciting physical phenomena varying from the excellent mixed ionic/electronic conduction behavior to the fascinating strong correlation and spin-state interactions.[5−9] In particular, $LaBaCo_2O_{5.5+\delta}$ (LBCO) has shown fast kinetics in oxidation−reduction reactions and unique magnetic and electric transport properties because of the existence of both A-site ordered and disordered structures. Furthermore, various intriguing physical phenomena have been observed because of the different oxidation states of cobalt ($Co^{2+}/Co^{3+}/Co^{4+}$) and electronic spin states.[10−15]

Recently, strain engineering in multifunctional thin-film materials has received considerable interest because of its significant impact on the microstructure and physical properties of epitaxial films.[16−21] Various new electrical and magnetic properties can be achieved by strain modification. Specifically, strain can significantly alter the transport behavior and magnetic properties of various perovskite cobaltate systems.[22−26] The strain in a film mainly arises from the lattice mismatch between the substrate and film and alters the Jahn−Teller distortion in the films. In-plane strain generally leads to an out-of-plane strain with a different sign. The lattice mismatch is also able to induce phase separation, sample inhomogeneities, interface dislocations, pseudoperiodic twinning, or formation of antiphase domains in the film[27−29] and to generate electronic and magnetic behavior not observed in the corresponding bulk material. Therefore, it is an important issue to study modification of the physical properties of LBCO thin films induced by lattice mismatch between the substrates and films. To systematically investigate the magnetic and magneto transport properties of LBCO on different substrates, we have deposited single-crystalline highly epitaxial LBCO thin films on (110) $NdGaO_3$ (NGO) for systematically studying their properties in comparison with the films on (001) $LaAlO_3$ (LAO), (001) $SrTiO_3$ (STO), and (001) MgO substrates. On different substrates, there are different interface strain values and induced lattice distortions, which can strongly influence the transport properties by changing the electron hopping. In this paper, we report a systematical study on various unusual physical phenomena induced by the lattice mismatch.

Received: November 5, 2013
Accepted: January 27, 2014
Published: January 27, 2014

EXPERIMENTAL SECTION

A KrF excimer pulsed-laser deposition system with a wavelength of 248 nm was employed to epitaxially grow LBCO thin films on an NGO substrate with the same optimized growth conditions as those for the films on the LAO, STO, and MgO substrates. Details can be found in previous reports.[8,11,12,30] Briefly, the optimal growth conditions have been determined to be at a deposition temperature of 850 °C and an oxygen pressure of 250 mTorr with a laser energy density of 2.0 J/cm^2. The thickness of the film was fixed at about 150 nm in order to keep the same thickness as those on the other three substrates. Soon after deposition, the LBCO films were in situ annealed at 850 °C for 15 min in a pure oxygen atmosphere at 200 Torr and slowly cooled to room temperature with a rate of 5 °C/min. The microstructure, crystallinity, and epitaxial behavior of the as-grown LBCO films were systematically examined by X-ray diffraction (XRD) and transmission electron microscopy (TEM). The transport behavior and magnetic properties of the thin films were evaluated using a Quantum Design Physical Property (PPMS-9) measurement system.

RESULTS AND DISCUSSION

XRD was employed to characterize the as-grown films to ensure the epitaxial quality. Figure 1 show X-ray θ–2θ scans and rocking-curve measurements for the LBCO films on MgO, LAO, NGO, and STO substrates.

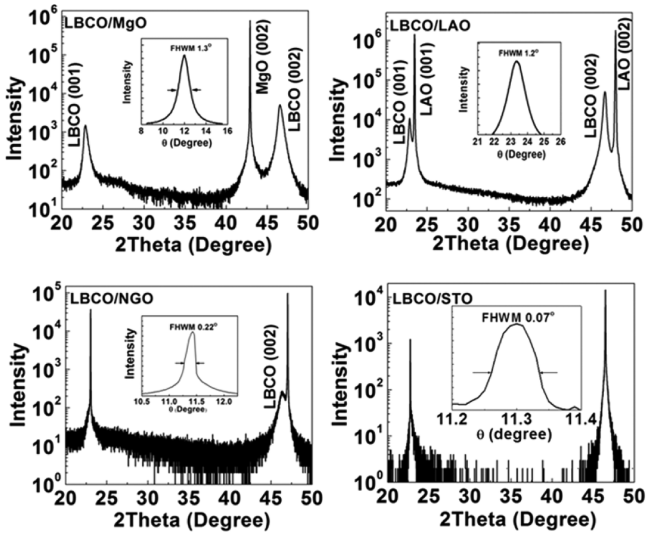

Figure 1. Typical XRD spectra of LBCO films on four different substrates. The insets are the FWHM plots of the films.

In a simple comparison, the disordered cubic structure of LBCO was used for microstructure characterization. Only the (00l) peaks appeared in the θ–2θ scan patterns for the films, and the peaks for the films on STO are overlapped with the corresponding peaks from the substrates due to very close lattice parameters, suggesting that the films on these substrates are c-axis-oriented. The rocking-curve measurements show that the full width at half-maximum (FWHM) values for the films on MgO, LAO, NGO, and STO substrates are 1.3°, 1.2°, 0.22°, and 0.07°,[12] respectively. The small FWHM values suggest that the as-grown LBCO films have good single crystallinity. The films on both MgO and LAO, however, show much larger FWHM values than those on NGO or STO, implying that the LBCO films are in a mosaic growth mode and may have numerous edge dislocations along the entire interfaces between the films and substrates.

Theoretically, the lattice mismatch between the film and substrate can be calculated by $\delta = (a_b - a_s)/a_s$ where a_s is the substrate lattice constant (provided by MTI Crystal Inc.) and a_b is the lattice constant of the LBCO bulk material, as shown in Table 1. For the (110) NGO substrate, the in-plane lattice constants are 3.858 and 3.868 Å along [001] and [1$\bar{1}$0], respectively. The transport behavior along these two directions is similar (Figure 4). In this paper, we focused on the investigation along [1$\bar{1}$0] because it generates the compressive strain with almost the same amplitude as the tensile strain induced by the STO substrate. According to the Bragg law, the out-of-plane lattice constants for the films on these four substrates can be determined from the reflection peak positions and are shown in Table 1. Clearly, the out-of-plane lattice constants on different substrates are different, indicating that there are different interface strains in the different films. On the basis of the constant unit cell volume model, the in-plane lattice constants of the films on different substrates can be calculated, as seen in Table 1. In the case of strained epitaxy, the in-plane lattice constant of the film can be estimated by the formula $a_b + (a_s - a_b)/2$ for the "tensile growth" and the formula $a_b - (a_b - a_s)/2$ for "compressed growth". Obviously, both in-plane and out-of-plane lattice constants for the films on MgO and LAO are very close to the bulk value, suggesting that the strains in the films on MgO and LAO are nearly fully relaxed. However, the in-plane lattice parameters for the LBCO films on STO and NGO calculated from the strained epitaxial model are very close to those calculated from the XRD measurements, indicating that the strains in these two films are not relaxed.

To further understand the nature of the strain effects induced by the lattice mismatch, cross-sectional TEM studies were used

Table 1. Lattice Constant and Lattice Mismatch/Interface Strain of the LBCO Film on Various Substrates

	lattice constant (Å)	lattice mismatch (%)	out-of-plane lattice constant (obsd)	out-of-plane strain (%)	in-plane lattice constant[a]	in-plane lattice constant[b]	in-plane strain (%)
bulk LBCO	3.886						
(001) LAO	3.792	2.48	3.890	0.10	3.884	3.839	−0.05
(110) NGO	3.868	0.47	3.907	0.54	3.876	3.877	−0.26
(001) STO	3.905	−0.49	3.870	−0.41	3.894	3.895	0.21
(001) MgO	4.20	−7.48	3.881	−0.13	3.889	4.043	0.08

[a]In-plane lattice constant obtained based on the constant unit cell volume model. [b]In-plane lattice constant according to the strained epitaxial thin-film model: $a_b + (a_s - a_b)/2$ for the case of STO and MgO, "tensile growth"; $a_b - (a_b - a_s)/2$ for the case of LAO and NGO, "compressed growth".

to study the epitaxial nature and interface microstructure of the LBCO films on various substrates.

Cross-sectional high-resolution TEM (HRTEM) images of LBCO films on MgO,[30] LAO,[8] NGO, and STO substrates are shown in Figure 2. Clearly, all of the films have excellent

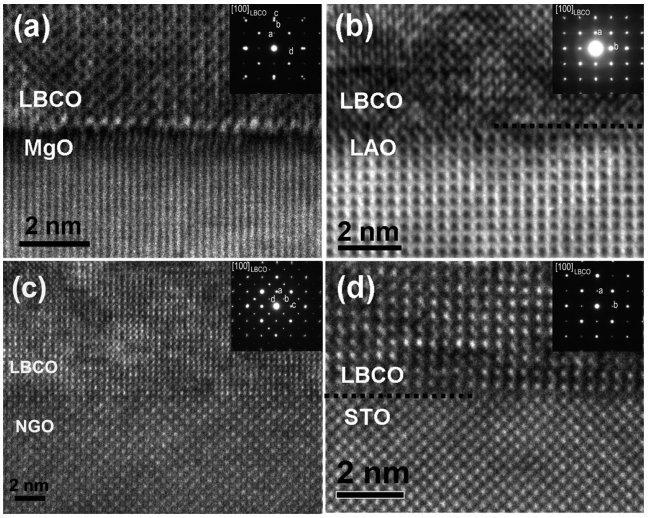

Figure 2. Cross-sectional HRTEM images showing the epitaxial behavior and interface structures of LBCO thin films on (a) MgO,[30] (b) LAO,[8] (c) NGO, and (d) STO substrates. The insets are the SAED patterns taken from the areas covering the interfaces between the films and substrates.

epitaxial quality with an atomically sharp interface. The insets in Figure 2 are the selected-area electron diffraction (SAED) patterns taken from the interface areas covering both the substrates and LBCO films. The indices of the labeled diffraction spots in the SAED patterns are listed in Table 2.

Table 2. Indices of the Diffraction Spots of the LBCO (Disordered) and Substrate in the SAED Pattern in Figure 2

sample	spot a	spot b	spot c	spot d
LBCO/MgO	(001) LBCO	(002) MgO	(002) LBCO	(010) LBCO
LBCO/LAO	(001) LBCO, (001) LAO	(010) LBCO// (010) LAO		
LBCO/NGO	(001) LBCO, (110) NGO	(010) NGO	(010) LBCO, ($\bar{1}$10) NGO	(100) NGO
LBCO/STO	(100) LBCO, (001) STO	(001) LBCO, (010) STO		

The sharp electron diffraction spots with no satellites or broadening further indicate that all of the LBCO thin films have good single crystallinity. As seen in Figure 2a,b, many edge dislocations are formed along the entire film/substrate interfaces for the films on MgO and LAO substrates, verifying the results from the X-ray studies that the strains in the films on these two substrates are fully relaxed by the formation of edge dislocations. However, no visible edge dislocations are found at the interfaces for the films on NGO and STO substrates, which is in good agreement with the XRD determination that the misfit strain is fully stored in the films because of the good lattice matches between the lattice parameters of the LBCO films and substrates.

Figure 3 is the temperature dependence of the magnetic moment from both zero-field-cooled (ZFC) and field-cooled

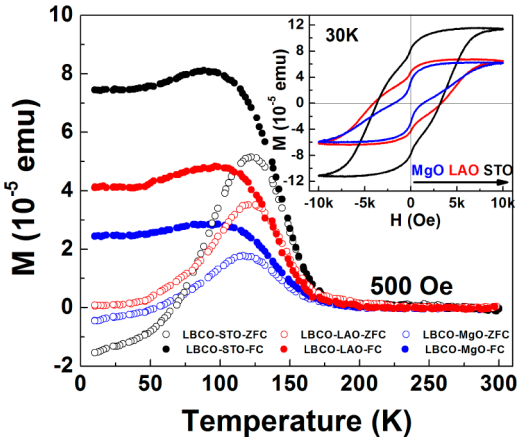

Figure 3. ZFC and FC magnetization of LBCO films on STO, LAO, and MgO substrates. The inset is the magnetic hysteresis for LBCO films on these three substrates measured at 30 K.

(FC) measurements under a 500 Oe magnetic field. Because the signal for the LBCO thin film on the NGO substrate is difficult to detect because of the large paramagnetic background from the NGO substrate, only the magnetic properties of LBCO/LAO, LBCO/STO, and LBCO/MgO are shown in the figure. The bifurcation between ZFC and FC below around 120 K is similar to the cluster glass behavior of the LBCO bulk material, resulting from the competition between randomly distributed ferromagnetic and antiferromagentic interactions.[23] Also, a negative magnetization was found at temperatures lower than 75 K in the ZFC measurement, similar to the effect from (La,Sr) CoO_3 thin films, resulting from the suppression of spin fluctuations.[1,31] Although the Curie temperature $T_c \sim 165$ K is itself reduced from the bulk value of 175 K because of the oxygen deficiency in all of the films, which caused a decrease in the doped hole density or destruction of the oxygen-hopping pathways.[32,33] Also, while T_c does not change under different film/substrate strains, the magnetic moments are found to decrease with an increase in the lattice mismatch. The LBCO film on STO shows the largest magnetic moment, while it has the smallest value on MgO. These magnetic phenomena can also be seen in the hysteresis loop measurements, as seen in the inset of Figure 3, showing the magnetic field dependence of the magnetic moment (m) at 30 K.

In principle, compressive strain will result in an increase in the ferromagnetic transition temperature because of reduction of the Co−O−Co bond length with a small increase in the Co−O−Co angle, while tensile strain produces the opposite effect.[25] However, it likely arises from variations due to lattice mismatch, such as different epitaxial strain states, antiphase domain, and phase separation.[34,35] On the other hand, although the thicknesses of the films are much larger than their critical thicknesses, the lattice distortion or antiphase domain may decrease the degree of ferromagnetic long-range order, resulting in a decrease in the magnetic moment. Furthermore, as seen in the hysteresis loops, each loop is a combination of two hysteresis loops that are the result of the nanoscale-ordered and disordered LBCO phases in the film. It is interesting to note that the nanoscale-ordered phase is dominant in the LBCO film with small strain, whereas the disordered phase is dominant in the film with large strain. These results are in good agreement with the previous studies of bulk materials.[14]

The temperature dependencies of the resistivity of the LBCO films on various substrates are shown in Figure 4. The transport

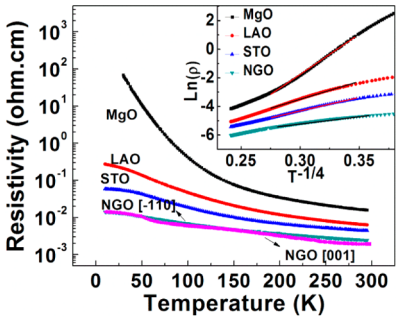

Figure 4. Temperature dependence of the resistivity for LBCO films on various substrates. The inset shows the log of the resistivity as a function of $T^{-1/4}$.

property measurements indicate that the resistivity $\rho(T)$ for the LBCO films increases exponentially with decreasing temperature in the entire measurement range from 290 to 10 K, indicating that all of the films possess semiconductor-like behavior.

However, it is noted that the resistivity for the LBCO thin film on MgO shows the highest resistivity value, followed by the films on LAO, STO, and NGO, in accordance with the sequence of lattice mismatch values. This evidence clearly indicates that the electrical transport properties of LBCO thin films are very sensitive to the interface lattice structures, although the interface strain energy is already fully released for the films on MgO and LAO by the formation of edge dislocations along the entire interface.

The interface strain values on STO (tensile) and NGO (compressive) are very close to each other, but the resistivity of the film on NGO is smaller than that on STO, indicating that the compressive strain can enhance the electronic conduction in the films, which is similar to traditional strain-effect behavior such as that in the $(La,Ca)MnO_3$ and $(La,Sr)CoO_3$ systems.[20,25] This phenomenon can be understood by the fact that the compressive strain may make the Co−O−Co bond length shorter, which causes charge carriers to more easily hop and enhances the conductivity of the LBCO film. The tensile strain decreases the electron-hopping amplitude, enhances the strength of the Jahn−Teller distortion, and then increases the localization of the carriers. On the other hand, the electrical transport properties of LBCO on MgO and LAO highly depend on the edge dislocation density and the antidomain boundary structures because the interface strain is fully released. Especially, the film on MgO may have plenty of antiphase domain boundaries because of surface step terrace induced antiphase domain formation.[36,37] Normally, the nanoscale-ordered and -disordered phases of LBCO has a Co−O−Co bond angle of 180° from 10 to 400 K, which permits overlapping of the Co 3d and O 2p orbitals. This type of linear bond angle is more facile for charge-carrier hopping resulting in semimetallic behavior.[14] It is possible that a larger interface strain induces a larger distortion of the Co−O−Co bond angle, leading to the higher resistivity.

In order to understand the electrical transport mechanism in the LBCO thin film, the measured resistivity is simulated by using $\rho(T) = \rho_0 e^{(T_0/T)^p}$ [$0 < p < 1$, $p = (d + 1)^{-1}$, where d is the spatial dimensionality, and T_0 is a characteristic temperature][38] and can be fitted very well with this equation when $p = {}^1/_4$, corresponding to a three-dimensional density of energy state. $\rho(T) = \rho_0 e^{(T_0/T)^p}$ reduces to Mott's variable-range-hopping model. In this model, $T_0 = (\beta/kN(E_F)L_{loc}{}^3)$, where L_{loc} is the localization length and β is a constant.[39] It is well-known that the optimal hopping distance, R, is

$$R = \left[\frac{9L_{loc}}{8\pi N(E_F)kT}\right]^{1/4}$$

and the corresponding energy difference between the final and initial hopping states (hopping energy) is $W = [4\pi R^3 N(E_F)/3]^{-1}$. Inserting the optimal hopping distance R into the hopping energy W, we get

$$W = \left[\frac{9\pi N(E_F)L_{loc}{}^3}{2k^3T^3}\right]^{-1/4} = \left[\frac{2k^4T^3T_0}{9\pi\beta}\right]^{1/4}$$

It is found that the hopping energy is proportional to T_0 at a fixed temperature. It is known that T_0 is proportional to the slope of a plot of $\ln(\rho)$ versus $T^{-1/4}$. From the plot (as shown in the inset of Figure 4), it is noted that the larger lattice mismatch induces the larger hopping energy, probably resulting from the density of edge dislocations at the interface and formation of the antiphase domain boundary.

Magnetoresistance (MR) studies were performed at different temperatures under an applied magnetic field perpendicular to the surface of film. The MR values were calculated by using MR (%) = $[\rho(H) - \rho(0)]/\rho(0) \times 100\%$, where $\rho(H)$ and $\rho(0)$ is the resistivity under the application of a magnetic field and without a magnetic field, respectively. In order to clearly compare the MR values on different substrates, the MR studies are summarized in Figure 5.

It is worth noting that the MR effect is almost isotropic for the temperature (160 and 100 K) near the Curie temperature, originating from suppression of spin fluctuations. However, at low temperature, the MR effect exhibits hysteresis effects, probably induced by the 90°-oriented nanodomains in the film. The MR values of the films on the four substrates at different temperatures under a 7 T magnetic field are shown in Figure 5e. The relationship between the MR effect and interface strain has a behavior similar to that of resistivity, and the MR values seem to increase with increasing lattice mismatch even though the strain is released at the interfaces for the films on MgO and LAO. The largest MR value of 43% at 40 K was found for the LBCO film on the MgO substrate in which the interface strain energy is fully released. This anomalous physical phenomenon of a giant MR effect, 5 times that from the corresponding bulk material measured at 50 K under a 7 T magnetic field,[14] can result from the formation of an antidomain boundary, a mosaic growth film structure, edge dislocation at the interface, and/or other defects. These will increase the scattering rate of the charge carrier in the film. Under the applied magnetic fields, spin scattering will be significantly reduced and the orientation of the domain can be modified, resulting in a decrease of the resistivity values and an increase of the conductivity, leading to the negative MR effect. On the other hand, the application of a magnetic field could align the spins of Co^{3+} and Co^{4+} along a parallel orientation, which would enhance the transfer integral of electron hopping from Co^{3+} to Co^{4+} due to the double exchange mechanism and then decrease the resistivity, leading to the negative MR.

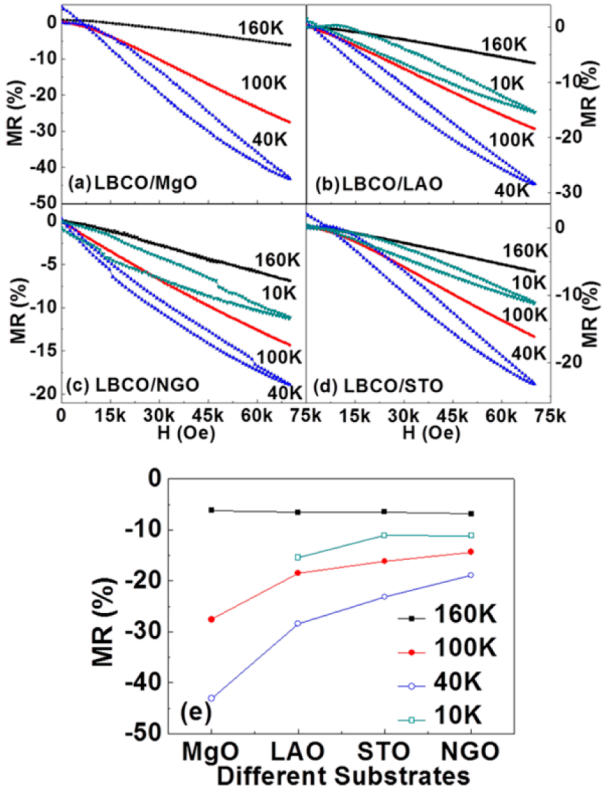

Figure 5. (a–d) MR as a function of the applied magnetic field at constant temperature on MgO,[30] LAO, NGO, and STO.[12] (e) MR on different substrates at 10, 40, 100, and 160 K under a 7 T magnetic field.

CONCLUSION

In summary, highly epitaxial LBCO thin films were successfully grown on MgO, LAO, NGO, and STO substrates by pulsed-laser deposition to investigate the influence of lattice mismatch induced by different substrates on the physical properties of the LBCO thin film. Microstructure investigations reveal that all of the LBCO films have excellent single-crystalline and epitaxial behavior with atomically sharp interfaces. Electrical transport and magnetic property measurements indicate that the film/substrate lattice mismatch can strongly affect the electrical conductivity, MR, and magnetic moment of the LBCO films. Specifically, the interface structures can significantly alter the MR and magnetic moments but not change the ferromagnetic transition temperature and so probably results from the strong coupling between the interface strain and nanodomain boundary and ordered oxygen vacancy structure. These new findings suggest that the electrical transport and magnetic properties can be controlled by the interface-induced strain, and this could be an important technique for new electromagnetic material design.

AUTHOR INFORMATION

Corresponding Author

*E-mail: cl.chen@utsa.edu.

Notes

The authors declare no competing financial interest.

ACKNOWLEDGMENTS

This research was partially supported by the National Science Foundation under Grant NSF-NIRT-0709293, the Department of Energy under Grants DE-FE0003780 and DE-SC0001284, and the State of Texas through the Texas Center for Superconductivity at the University of Houston and the National Science Foundation of China under Grants NSFC-11028409, 51202185, and 11329402. A.J.J. also acknowledges support from the Robert A Welch Foundation (Grant E-0024). M.L. and C.R.M. acknowledge support from the "China Scholarship Council" for their Ph.D. studies at the University of Texas at San Antonio.

REFERENCES

(1) Luo, G. P.; Wang, Y. S.; Chen, S. Y.; Heilman, A. K.; Chen, C. L.; Chu, C. W.; Liou, Y.; Ming, N. B. *Appl. Phys. Lett.* **2000**, *76*, 1908–1910.
(2) Taskin, A. A.; Lavrov, A. N.; Ando, Y. *Phys. Rev. B* **2005**, *71*, 134414.
(3) Taskin, A. A.; Lavrov, A. N.; Ando, Y. *Appl. Phys. Lett.* **2005**, *86*, 091910.
(4) De Souza, R. A.; Kilner, J. A. *Solid State Ionics* **1998**, *106*, 175–187.
(5) Fauth, F.; Suard, E.; Caignaert, V.; Domenges, B.; Mirebeau, I.; Keller, L. *Eur. Phys. J. B* **2001**, *21*, 163–174.
(6) Kim, G.; Wang, S.; Jacobson, A. J.; Yuan, Z.; Donner, W.; Chen, C. L.; Reimus, L.; Brodersen, P.; Mims, C. A. *Appl. Phys. Lett.* **2006**, *88*, 024103.
(7) Kundu, A. K.; Rautama, E. L.; Boullay, P.; Caignaert, V.; Pralong, V.; Raveau, B. *Phys. Rev. B* **2007**, *76*, 184432.
(8) Liu, J.; Collins, G.; Liu, M.; Chen, C. L.; Jiang, J. C.; Meletis, E. I.; Zhang, Q. Y.; Dong, C. A. *Appl. Phys. Lett.* **2010**, *97*, 094101.
(9) Yuan, Z.; Liu, J.; Chen, C. L.; Wang, C. H.; Luo, X. G.; Chen, X. H.; Kim, G. T.; Huang, D. X.; Wang, S. S.; Jacobson, A. J.; Donner, W. *Appl. Phys. Lett.* **2007**, *90*, 212111.
(10) Kundu, A. K.; Raveau, B.; Caignaert, V.; Rautama, E. L.; Pralong, V. *J. Phys.: Condens. Matter* **2009**, *21*, 056007.
(11) Liu, J.; Liu, M.; Collins, G.; Chen, C. L.; Jiang, X. N.; Gong, W. Q.; Jacobson, A. J.; He, J.; Jiang, J. C.; Meletis, E. I. *Chem. Mater.* **2010**, *22*, 799–802.
(12) Liu, M.; Liu, J.; Collins, G.; Ma, C. R.; Chen, C. L.; He, J.; Jiang, J. C.; Meletis, E. I.; Jacobson, A. J.; Zhang, Q. Y. *Appl. Phys. Lett.* **2010**, *96*, 132106.
(13) Ma, C. R.; Liu, M.; Collins, G.; Liu, J.; Zhang, Y. M.; Chen, C. L.; He, J.; Jiang, J. C.; Meletis, E. I. *Appl. Phys. Lett.* **2012**, *101*, 021602.
(14) Rautama, E. L.; Boullay, P.; Kundu, A. K.; Caignaert, V.; Pralong, V.; Karppinen, M.; Raveau, B. *Chem. Mater.* **2008**, *20*, 2742–2750.
(15) Rautama, E. L.; Caignaert, V.; Boullay, P.; Kundu, A. K.; Pralong, V.; Karppinen, M.; Ritter, C.; Raveau, B. *Chem. Mater.* **2009**, *21*, 102–109.
(16) Grutter, A.; Wong, F.; Arenholz, E.; Liberati, M.; Suzuki, Y. *J. Appl. Phys.* **2010**, *107*, 09E138.
(17) Grutter, A.; Wong, F.; Arenholz, E.; Liberati, M.; Vailionis, A.; Suzuki, Y. *Appl. Phys. Lett.* **2010**, *96*, 082509.
(18) Lin, Y.; Dai, C.; Li, Y. R.; Chen, X.; Chen, C. L.; Bhalla, A.; Jia, Q. X. *Appl. Phys. Lett.* **2010**, *96*, 102901.
(19) Park, S.; Ryan, P.; Karapetrova, E.; Kim, J. W.; Ma, J. X.; Shi, J.; Freeland, J. W.; Wu, W. D. *Appl. Phys. Lett.* **2009**, *95*, 072508.
(20) Xiong, Y. M.; Wang, G. Y.; Luo, X. G.; Wang, C. H.; Chen, X. H.; Chen, X.; Chen, C. L. *J. Appl. Phys.* **2005**, *97*, 083909.
(21) Yang, F.; Kemik, N.; Biegalski, M. D.; Christen, H. M.; Arenholz, E.; Takamura, Y. *Appl. Phys. Lett.* **2010**, *97*, 092503.
(22) Donner, W.; Chen, C. L.; Liu, M.; Jacobson, A. J.; Lee, Y. L.; Gadre, M.; Morgan, D. *Chem. Mater.* **2011**, *23*, 984–988.
(23) Nakajima, T.; Ichihara, M.; Ueda, Y. *J. Phys. Soc. Jpn.* **2005**, *74*, 1572–1577.
(24) Torija, M. A.; Sharma, M.; Fitzsimmons, M. R.; Varela, M.; Leighton, C. *J. Appl. Phys.* **2008**, *104*, 023901.
(25) Xie, C. K.; Budnick, J. I.; Hines, W. A.; Wells, B. O.; Woicik, J. C. *Appl. Phys. Lett.* **2008**, *93*, 182507.

(26) Xiong, Y. M.; Chen, T.; Wang, G. Y.; Chen, X. H.; Chen, X.; Chen, C. L. *Phys. Rev. B* **2004**, *70*, 094407.
(27) Babushkina, N. A.; Belova, L. M.; Khomskii, D. I.; Kugel, K. I.; Gorbenko, O. Y.; Kaul, A. R. *Phys. Rev. B* **1999**, *59*, 6994−7000.
(28) Biswas, A.; Rajeswari, M.; Srivastava, R. C.; Li, Y. H.; Venkatesan, T.; Greene, R. L.; Millis, A. J. *Phys. Rev. B* **2000**, *61*, 9665−9668.
(29) Zhang, L. W.; Israel, C.; Biswas, A.; Greene, R. L.; de Lozanne, A. *Science* **2002**, *298*, 805−807.
(30) Liu, M.; Ma, C. R.; Liu, J.; Collins, G.; Chen, C. L.; He, J.; Jiang, J. C.; Meletis, E. I.; Sun, L.; Jacobson, A. J.; Whangbo, M. H. *ACS Appl. Mater. Interfaces* **2012**, *4*, 5524−5528.
(31) Kwon, C.; Gim, Y.; Fan, Y.; Hundley, M. F.; Roper, J. M.; Arendt, P. N.; Jia, Q. X. *Appl. Phys. Lett.* **1998**, *73*, 695−697.
(32) Dho, J.; Hur, N. H.; Kim, I. S.; Park, Y. K. *J. Appl. Phys.* **2003**, *94*, 7670−7674.
(33) Xie, C. K.; Budnick, J. I.; Wells, B. O. *Appl. Phys. Lett.* **2007**, *91*, 172509.
(34) Biswas, A.; Rajeswari, M.; Srivastava, R. C.; Venkatesan, T.; Greene, R. L.; Lu, Q.; de Lozanne, A. L.; Millis, A. J. *Phys. Rev. B* **2001**, *63*, 184424.
(35) Campillo, G.; Berger, A.; Osorio, J.; Pearson, J. E.; Bader, S. D.; Baca, E.; Prieto, P. *J. Magn. Magn. Mater.* **2001**, *237*, 61−68.
(36) Chen, C. L.; Shen, J.; Chen, S. Y.; Luo, G. P.; Chu, C. W.; Miranda, F. A.; Van Keuls, F. W.; Jiang, J. C.; Meletis, E. I.; Chang, H. Y. *Appl. Phys. Lett.* **2001**, *78*, 652−654.
(37) Jiang, J. C.; Lin, Y.; Chen, C. L.; Chu, C. W.; Meletis, E. I. *J. Appl. Phys.* **2002**, *91*, 3188−3192.
(38) I., S. B.; L., E. A. Springer-Verlag: Berlin, 1984.
(39) Celik Butler, Z.; Shan, P. C.; Butler, D. P.; Jahanzeb, A.; Travers, C. M.; Kula, W.; Sobolewski, R. *Solid-State Electron.* **1997**, *41*, 895−899.